Synthesis, crystal structure, vibrational spectral analysis and Z-scan studies of a new organic crystal N,N′dimethylurea ninhydrin: A scaled quantum mechanical force field study

ARTICLE · SEPTEMBER 2015

DOI: 10.1016/j.optmat.2015.08.002

Optical Materials 48 (2015) 233–242

Contents lists available at ScienceDirect

Optical Materials

journal homepage: www.elsevier.com/locate/optmat

Synthesis, crystal structure, vibrational spectral analysis and Z-scan studies of a new organic crystal N,N′dimethylurea ninhydrin: A scaled quantum mechanical force field study

Jerin Susan John [a], D. Sajan [a,*], T. Umadevi [b], K. Chaitanya [c], Pranitha Sankar [d], Reji Philip [d]

[a] Department of Physics, Bishop Moore College, Mavelikara, 690110 Kerala, India
[b] Department of Physics, Government Arts College for Women (Autonomous), Pudukottai, India
[c] Department of Chemistry, Nanjing University of Science and Technology, Xialingwei 200, Nanjing, People's Republic of China
[d] Light and Matter Physics Group, Raman Research Institute, C.V. Raman Avenue, Sadashiva Nagar, Bangalore 560080, India

ARTICLE INFO

Article history:
Received 16 January 2015
Received in revised form 12 July 2015
Accepted 3 August 2015
Available online 12 August 2015

Keywords:
X-ray diffraction
FT-IR and FT-Raman
Quantum mechanical method of computation
NBO
Nonlinear optical materials

ABSTRACT

A new organic material, N,N′dimethylurea ninhydrin (3a,8a-dihydroxy-1,3-dimethyl-1,3,3a,8a-tetrahydroindeno[2,1-d]imidazole-2,8-dione) (NDUN) was synthesized. Structural details were obtained from single crystal X-ray diffraction (XRD) data. A detailed interpretation of the vibrational spectra is carried out with the aid of normal coordinate analysis following the scaled quantum mechanical force field methodology. TG/DTA and ^{1}H NMR studies were carried out. Linear optical properties were studied from UV–Vis spectra. From the open aperture Z-scan data, it is found that the molecule shows third order nonlinear optical behaviour due to two photon absorption (2PA) mechanism.

1. Introduction

Due to wide variety of applications in the field of photonic technologies, nonlinear optical (NLO) materials have been continuously attracting the attention of researchers. NLO properties such as fast response time and large third-order non-linearity $\chi^{(3)}$ are essential for optical data storage, optical information processing, harmonic generation, optical switching, optical communication, and optical limiting applications [1]. Organic materials have many advantages over inorganic materials in NLO applications, due to their large chemical flexibility, high conjugated framework, ease of design, large nonlinearities and fast response times.

Urea plays an important role in organic crystal engineering [2]. It is a useful NLO material which has a high optical transparency (to 200 nm), large damage threshold (1–5 GW/cm^2) and an extraordinary birefringence. Urea was the first organic material in which optical parametric amplification was demonstrated [3]. And some of its derivatives also exhibited promising NLO properties. For example, N,N′dimethylurea crystallizes in the orthorhombic system and exhibited second-harmonic generation and led to the formation of various coordination compounds. Ninhydrin (2,2-dihydroxy-1,3-indanedione), whose derivative is the present case of study, is an organic material crystallizing in a monoclinic crystal system which represents a class of carbonyl compounds with reactive keto group. Based on the chemical structure and its potential to generate hydroxyl radicals, ninhydrin has been described as an analytical tool in various fields [4] such as pharmacology, forensic investigation, chemistry and food sciences Ninhydrin is widely used to detect fingerprints and also to detect primary or secondary amines. Investigations on NLO effects were initially focused on pure ninhydrin and later on its urea derivative, which provided crystalline materials with good thermal, chemical, and mechanical stabilities.

In the present study, for the first time we report the synthesis, crystal growth, X-ray diffraction, Nuclear Magnetic Resonance (NMR), FT-IR and FT-Raman spectra, and Z-scan studies of N,N′dimethylurea ninhydrin (3a,8a-dihydroxy-1,3-dimethyl-1,3,3a,8a-tetrahydroindeno[2,1-d]imidazole-2,8-dione) (NDUN), using both theoretical and experimental techniques. Detailed vibrational spectral investigations of NDUN molecule using scaled quantum mechanical (SQM) force field technique based on density functional theory (DFT) calculations is performed. From natural bond orbital analysis (NBO), electron charge transfer through

* Corresponding author.
E-mail address: dsajanbmc@gmail.com (D. Sajan).

http://dx.doi.org/10.1016/j.optmat.2015.08.002
0925-3467/

intermolecular hydrogen bonding is explained. The molecular structure of NDUN molecule is shown in Fig. 1(a).

2. Experimental procedure

2.1. Synthesis and crystal growth

The chemicals are commercially available in AR grade and are used without further purification. The title compound was synthesized by heating an aqueous solution of N,N′-dimethylurea and ninhydrin in equimolar amounts. The first step in the reaction process involves the nucleophilic addition of N,N′-dimethylurea to ninhydrin carbonyl group. The product so obtained undergoes intramolecular condensation with the elimination of water molecule in the second step and thus forms the product. (Scheme that depicts the probable mechanistic pathway of formation of NDUN is given in Supplementary Data.) The further purification of the synthesized compound was done by successive recrystallization and used for crystal growth. NDUN is soluble in acetone, DMF, methanol, ethanol and DMSO, but solubility in DMF was found to promote the reasonable rate of crystal growth of NDUN single crystals. (As-grown NDUN crystals from DMF by solvent evaporation method are shown in Fig. S1 in Supplementary Material.)

2.2. X-ray diffraction, FT-IR, FT- Raman, NMR, UV–Vis spectra and thermal studies

To determine the molecular structure of a crystal, the data of single crystal XRD of NDUN is collected using a Stoe Image Plate Diffraction system at 173 K, equipped with a two-circle goniometer and using Mo Kα graphite monochromated radiation (Image plate distance 100 mm, ω rotation scans 0–180° at φ 0°, and 0–180.0° at φ 90°, step $\Delta\omega = 1.0°$, exposures of 2 min per image, 2θ range 2.29–59.53°, $d_{min} - d_{max} = 17.779 - 0.716$ Å.) The structure was solved and refined using the programs SHELXS and SHELXL, respectively. The crystalline perfection of the specimen crystal is evaluated using high-resolution X-ray diffraction (HRXRD) analysis. A multicrystal X-ray diffractometer developed at National Physical Laboratory (NPL), New Delhi was used to record high-resolution rocking or diffraction curves (DCs). The detector was kept at the same angular position $2\theta_B$ with wide opening for its slit, the so-called ω scan [5]. The Bragg's law gives the correlation between the minimum distance between parallel planes d and the angular position of the X-Ray peak in the two theta–omega scan.

The FT-IR spectrum of the solid was recorded in the wavenumber range from 4000 to 400 cm^{-1} with a Bruker Alpha spectrophotometer equipped with a Globar source and deuterated triglycine sulfate (DGTS) detector. The data were collected at 1 cm^{-1} resolution and the spectrum was enhanced by the accumulation of 200 scans. The Raman spectrum of the solid compound was recorded between 4000 and 10 cm^{-1} with a Bruker RF100/S spectrometer equipped with an Nd:YAG laser (excitation line of 1064 nm, 800 mW of laser power) and a Ge detector cooled to liquid nitrogen temperature. The spectrum was recorded with a resolution of 2 cm^{-1} and 200 scans. The UV–Vis absorption spectrum of the sample was recorded in ethanol solution using a Shimadzu UV–Vis spectrophotometer in the spectral region of 200–1100 nm. The ^1H NMR spectral analyses were carried out for the NDUN crystal sample in deuterated solvent of chloroform ($CDCl_3$) using Bruker AC 200-NMR spectrometer. The differential scanning calorimetry measurements were performed on a METTLER-TOLEDO DSC 1 apparatus equipped with the low temperature attachment. Heating and cooling scans were carried out at 5 °C/min rates in the −80 °C to 180 °C temperature range. The powdered sample taken in aluminium pans weighed 2.92 mg.

2.3. Nonlinear optical studies: Z-scan measurement

The optical nonlinearity measurements were carried out using laser pulses of 5 ns duration (λ = 532 nm, second harmonic output of Nd:YAG laser), employing the technique of open aperture Z-scan [6], in which the optical transmission of the sample is measured as a function of input laser fluence. Different fluences are obtained by keeping the sample at different positions with respect to the focal point of a focused laser beam. Beam propagation direction is taken as the z-axis and the focal point is taken as z = 0. The sample is loaded on a translation stage and moved from one side of the focus to the other through many small steps, with the transmission being measured at each step. The nature of the absorptive nonlinearity in the system is revealed in the graph plotted between sample position z and the normalized transmittance of the sample, known as the open-aperture Z-scan curve [7]. If a spatially Gaussian laser beam is used for excitation, then each z-position will correspond to an input laser fluence of $4(\ln 2)^{1/2}E_{in}/\pi^{3/2}\omega(z)^2$, where E_{in} is the input laser pulse energy and ω(z) is the beam radius. ω(z) is given by

$$\omega(z) = \omega(0) \times \left[1 + (z/z_0)^2\right]^{1/2} \quad (1)$$

where ω(0) is the beam radius at the focus and $z_0 = \pi\omega(0)^2/\lambda$ is the Rayleigh range (diffraction length), where λ is the excitation wavelength. From the open aperture Z-scan data it is possible to

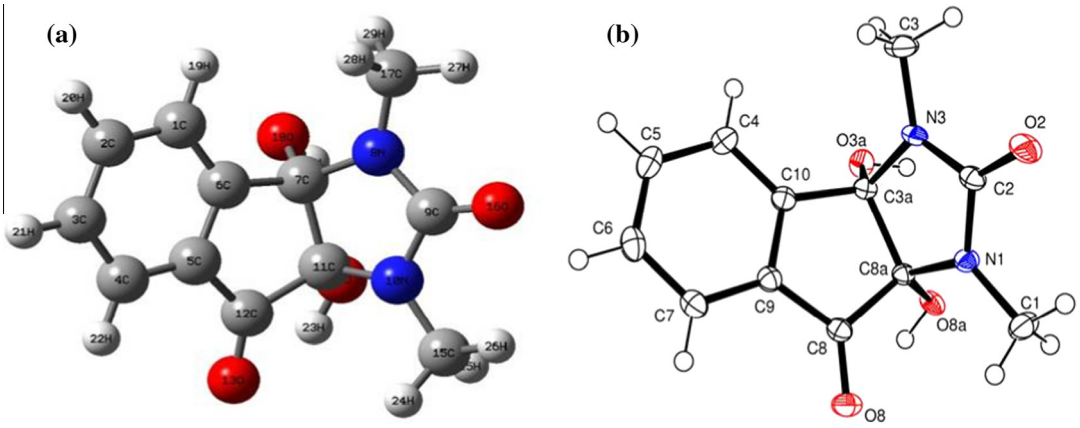

Fig. 1. (a) NDUN molecule and (b) the molecular structure of NDUN and the crystallographic numbering scheme (50% probability displacement ellipsoids).

plot a graph between the input laser fluence and the sample transmission, which is known as the nonlinear transmission curve.

3. Computational details

All the calculations in this paper were performed with the Gaussian 09W program [8]. Geometry optimization of NDUN is performed using the Becke, three-parameter, Lee–Yang–Parr (B3LYP) functional [9,10] supplemented with standard cc-pVTZ basis set (referred to as DFT calculations). The NBO calculation was performed using the NBO 5.0 [11–13] program as implemented in the Gaussian 09 package. Following the Scaled Quantum Mechanical Force Field (SQMFF) procedure [14], the harmonic force field for NDUN molecule was evaluated at the B3LYP/cc-pVTZ level. The resulting force fields were transformed to 'natural' internal coordinates by using the MOLVIB 7.0 program [15,16]. The natural internal coordinates for NDUN have been defined as proposed by Fogarasi et al., [17] while the ring coordinates were defined as in Pulay et al. [18,19].

Theoretical optical studies of NDUN were done using the TD-DFT method. In this method, energies, oscillator strengths of electronic singlet-singlet transitions and the absorption wavelengths were calculated. Polarizable continuum model (PCM) has been used to involve solvent effects.

The NLO properties of a molecule can be measured theoretically by calculating the hyperpolarizability values. The measure of second order NLO response can be obtained from the first hyperpolarizability values. First hyperpolarizability (β) third rank tensor, described by a $3 \times 3 \times 3$ matrix, contains 27 components, but due to Kleinman symmetry the components are reduced to 10 [20]. The Gaussian'09 output gives the 10 components of β such as β_{xxx}, β_{yxx}, β_{xyy}, β_{yyy}, β_{zxx}, β_{xyx}, β_{zyy}, β_{xzz}, β_{yzz} and β_{zzz}. The components of the first hyperpolarizability can be calculated using the following equation:

$$\beta_i = \beta_{iii} + \frac{1}{3}\sum_{i \neq j}(\beta_{ijj} + \beta_{jij} + \beta_{jji}) \quad (2)$$

Using the x, y and z components of β, the magnitude of the first hyperpolarizability tensor can be calculated from Gaussian'09W output by using the equation

$$\beta = \left(\beta_x^2 + \beta_y^2 + \beta_z^2\right)^{1/2} \quad (3)$$

where $\beta_x = \beta_{xxx} + \beta_{xyy} + \beta_{xzz}$, $\beta_y = \beta_{yyy} + \beta_{yzz} + \beta_{yxx}$ and $\beta_z = \beta_{zzz} + \beta_{zxx} + \beta_{zyy}$. The result obtained in atomic units (a.u.) can be converted to electrostatic unit units (e.s.u.) using the relation, 1 a.u. = 8.6393×10^{-33} e.s.u.

The number of independent components of the fourth rank second hyperpolarizability tensor depends on the crystal classes. For triclinic system, there are 81 independent non-zero elements which are reduced by Kleinman symmetry. The second hyperpolarizability value is calculated using the equation [21],

$$\langle\gamma\rangle = \frac{1}{5}\left(\gamma_{xxxx} + \gamma_{yyyy} + \gamma_{zzzz} + 2\gamma_{xxyy} + 2\gamma_{xxzz} + 2\gamma_{yyzz}\right) \quad (4)$$

The molecular linear polarizability calculation can be done using the relation,

$$\langle\alpha\rangle = \frac{1}{3}\left(\alpha_{xx} + \alpha_{yy} + \alpha_{zz}\right) \quad (5)$$

where α_{xx}, α_{yy} and α_{zz} are the matrix components of second rank polarizability tensor. There are no vanishing components in the matrix for triclinic crystals. The polarizability and hyperpolarizabilities of NDUN were calculated using B3LYP/6-311++G(d,p) basis set based on the finite-field approach.

4. Results and discussion

4.1. X-ray diffraction studies

The molecular structure of NDUN with 50% probability displacement ellipsoid [22] is shown in Fig. 1(b). The molecular structure consists of three rings, namely benzene, cyclopentane and imidazole. The mean planes of the cyclopentane ring and the benzene ring are inclined to one another by 1.70(8)°. However, the mean-plane of the imidazole ring is inclined to the mean planes of the cyclopentane ring and the benzene ring by 64.18(8)° and 64.19(8)° respectively. The crystal data and the refinement details are given in Table 1. The molecular structure is stabilized by strong O—H···O hydrogen bonds and weaker C—H···O interactions (Table 2). (The crystal packing of NDUN with the O—H···O and C—H···O hydrogen bonds drawn using the software Mercury is shown in Figs. S2(a) and S2(b) in Supplementary Material.)

Powder X-ray diffraction patterns were recorded using powder X-ray diffractometer with Cu Kα1 radiation (λ = 1.54060 Å). Finely crushed powder of NDUN crystal was scanned in the 2θ values ranging from 20° to 60° and the corresponding peaks were indexed (Fig. 2a). Fig. 2b shows the RC recorded for a NDUN crystal grown using (0 1 1) diffracting planes in symmetrical Bragg geometry. As seen in Fig. 2b, the curve does not have a single diffraction peak.

Table 1
Crystallographic data and refinement details for NDUN.

Formula	C_{12} H_{12} N_2 O_4
Formula weight	248.24
Crystal system	Triclinic
Space group	P-1 (no. 2)
a (Å)	6.8976(6)
b (Å)	8.4603(7)
c (Å)	10.5958(9)
α (°)	104.876(7)
β (°)	90.788(7)
γ (°)	108.696(6)
V (Å^3)	562.94(8)
Z	2
D_{calc} (g cm^{-3})	1.464
F (000)	260
μ (cm^{-1})	1.12
Crystal size (mm)	0.42 × 0.28 × 0.15
Colour, shape	Colourless, plate
θ_{min}, θ_{max} (°)	2.0, 29.18
Measured refln.	11,049
Unique refln., R_{int}	3047, 0.048
Obs. refln. [$I > 2\sigma$ (I)]	2321
No. refined parameters	174
R1[a] (obs. refln.), wR2[b] (all refln.)	0.047, 0.1083
S[c]	1.016
Min. and max. resd. dens. (e/Å^3)	−0.275, 0.332

[a] $R1 = [\Sigma|F_o| - |F_c|]/\Sigma|F_o|$ (based on F);
[b] $wR2 = [[\Sigma w(|F_o^2 - F_c^2|)2]/[\Sigma w(F_o^2)^2]]^{1/2}$ (based on F^2),
[c] $GOF = ((\Sigma(|F_o| - |F_c|)2)/(N_o - N_v))^{1/2}$ with N_o = number of observed reflections and N_v = number of parameter.

Table 2
Hydrogen bond geometry (Å).

D—H···A	D—H	H···A	D···A	D—H···A
O3a—H3aO···O8a[a]	0.91(2)	1.86(2)	2.7547(16)	169(3)
O8a—H8aO···O2[b]	0.88(3)	1.74(3)	2.6042(17)	165(2)
C1—H1B···O8[c]	0.98	2.56	3.369(2)	140
C5—H5···O8[d]	0.95	2.51	3.423(2)	162

Symmetry codes:
[a] −x + 1, −y + 1, −z++.
[b] x − 1, y, z.
[c] −x + 1, −y + 1, −z.
[d] x, y − 1, z.

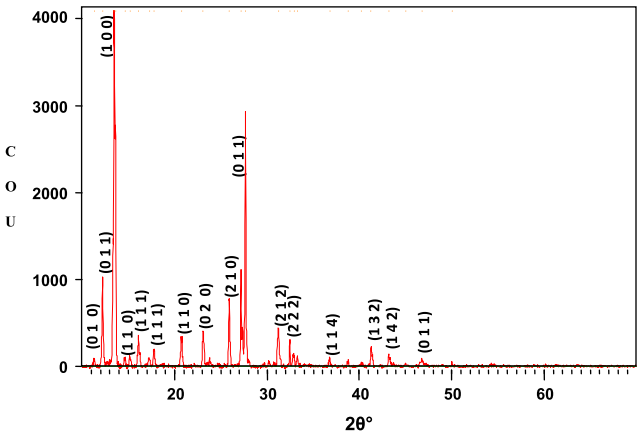

Fig. 2a. Powder X-ray diffraction of NDUN crystal.

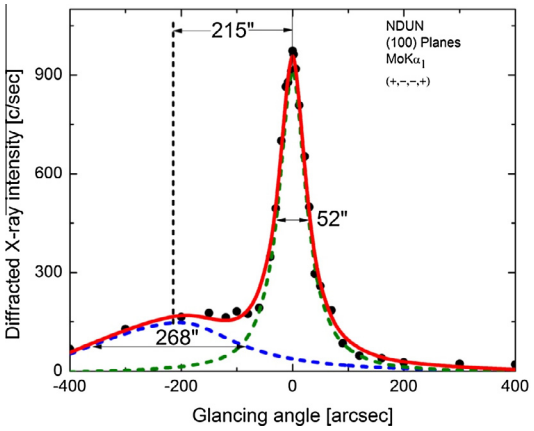

Fig. 2b. Rocking curve recorded for a typical GAC single crystal grown by SEST-method using ethanol as solvent for (0 1 1) diffracting planes.

The solid line, which follows well with the experimental points (filled circles), is the convoluted curve of two peaks using the Lorentzian fit. The additional peak depicts an internal structural very low angle (tilt angle $\leqslant 1$ arcmin) boundary [23] whose tilt angle (misorientation angle between the two crystalline regions on both sides of the structural grain boundary) is 60 arcsec from its adjoining region. The FWHM (full width at half maximum) of the main peak and the low angle boundary are respectively 27 and 130 arcsec. Though the crystal contains a low angle boundary, the low angular spread of ~400 arcsec of the RC indicates that the quality of the crystal is fairly good. The low intensity and the broadness of the curve belonging to the low angle boundary reveals that a small portion of this region is having small mosaic blocks which are mis-oriented by few tens of arcsec. It may be mentioned here that such a very low angle boundary could be detected with well-resolved peak in the diffraction curve only because of the high-resolution of the multicrystal X-ray diffractometer used in the present study. The influence of such defects may not influence much on the NLO properties. However, a quantitative analysis of such unavoidable defects is of great importance, particularly in case of phase matching applications [24].

4.2. NMR spectral study

The Nuclear Magnetic Resonance (NMR) spectrum confirms the presence of different types of protons present in the molecule, by using the magnetic properties of the atomic nuclei. Energy required to bring a nucleus into resonance is proportional to the electromagnetic radiation frequency, and it is the resonance frequencies that are plotted on an NMR spectrum [25]. The recorded ^{1}H NMR spectrum is shown in Fig. 3. The two intense proton signals exhibited at δ 2.759 and δ 2.847 ppm have been assigned to two sets of chemically and magnetically distinct methyl protons of C1 and C3 methyl groups respectively (Fig. 1(b)). The two OH protons one each on 3a and 8a oxygen atoms appear at $\delta = 2.07$ and 3.35 ppm respectively. Four proton signals appearing in the aromatic region of the spectrum owe to C5, C6, C7 and C4 aromatic protons in the ninhydrin moiety.

4.3. Optimized geometry

According to the atom numbering shown in Fig. 1(a), the experimental and theoretical structure parameters of NDUN, obtained from X-ray diffraction data and Gaussian'09 program package using the B3LYP/cc-pVTZ basis set respectively, are compared and Table 3 shows the results. The CC bond lengths of 1.39 Å which is between 1.54 Å for C—C single bond and 1.34 Å for C=C double bond confirms electron delocalization. The bond length of C_7—C_{11} in NDUN is increased to 1.57 Å from 1.54 Å for ninhydrin molecule due to the attachment of N,N′dimethylurea. There is a considerable shortening of C—O single bonds in the molecule. C_7—O_{18} and C_{11}—O_{14} single bonds have a length of 1.40 Å which is less than

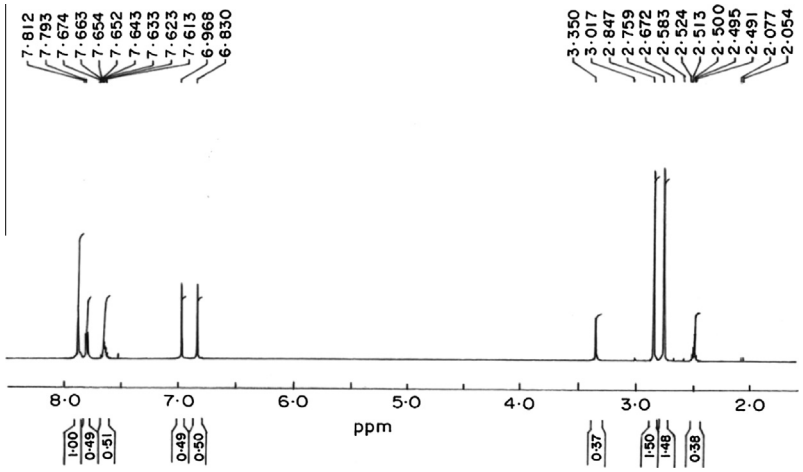

Fig. 3. ^{1}H NMR spectrum of NDUN.

Table 3
Optimized geometric parameters of NDUN.

Bond lengths (Å)			Bond angles (°)			Dihedral angles (°)		
Parameter	Theoretical	XRD	Parameter	Theoretical	XRD	Parameter	Theoretical	XRD
C_1—C_2	1.3903	1.387	C_6—C_1—H_{19}	121.14	120.76	H_{19}—C_1—C_2—H_{20}	−1.11	−0.65
C_2—C_3	1.3985	1.401	H_{19}—C_1—C_2	120.25	120.78	H_{19}—C_1—C_2—C_3	178.34	179.34
C_3—C_4	1.3845	1.383	C_2—C_1—C_6	118.58	118.46	C_1—C_2—C_3—H_{21}	−179.85	−179.31
C_4—C_5	1.3935	1.394	C_1—C_2—C_3	121.34	121.31	C_1—C_2—C_3—C_4	−0.45	0.68
C_5—C_6	1.3963	1.400	C_1—C_2—H_{20}	119.38	119.35	H_{20}—C_2—C_3—H_{21}	−0.38	0.68
C_1—C_6	1.3888	1.392	H_{20}—C_2—C_3	119.26	119.34	H_{20}—C_2—C_3—C_4	179.01	−179.32
C_1—H_{19}	1.0803	0.949	C_2—C_3—C_4	120.24	120.52	C_2—C_3—C_4—H_{22}	−178.82	179.57
C_2—H_{20}	1.0819	0.950	C_2—C_3—H_{21}	119.59	119.75	C_2—C_3—C_4—C_5	0.92	−0.40
C_3—H_{21}	1.0813	0.950	H_{21}—C_3—C_4	120.15	119.72	C_3—C_4—C_5—C_6	−0.43	0.08
C_4—H_{22}	1.0813	0.950	C_3—C_4—H_{22}	121.65	120.88	C_3—C_4—C_5—C_{12}	−175.75	−175.91
C_5—C_{12}	1.4675	1.469	C_3—C_4—C_5	118.29	118.22	H_{21}—C_3—C_4—H_{22}	0.57	−0.44
C_6—C_7	1.5239	1.513	H_{22}—C_4—C_5	120.05	120.91	H_{21}—C_3—C_4—C_5	−179.67	179.59
C_{12}═O_{13}	1.2120	1.215	C_4—C_5—C_{12}	127.95	127.94	H_{22}—C_4—C_5—C_6	179.31	−179.89
C_{12}—C_{11}	1.5396	1.545	C_4—C_5—C_6	121.65	121.44	H_{22}—C_4—C_5—C_{12}	3.99	4.12
C_7—C_{11}	1.5700	1.583	C_6—C_5—C_{12}	110.25	110.51	C_4—C_5—C_6—C_1	−0.54	−0.02
C_7—O_{18}	1.4003	1.396	C_5—C_6—C_1	119.86	120.05	C4—C5—C6—C7	−178.91	179.94
O_{18}—H_{30}	0.9684	0.911	C_5—C_6—C_7	111.80	112.05	C_5—C_6—C_1—H_{19}	−177.85	−179.67
C_{11}—O_{14}	1.4083	1.398	C_1—C_6—C_7	128.31	127.91	C_5—C_6—C_1—C_2	1.01	0.28
O_{14}—H_{23}	0.9669	0.882	C_6—C_7—C_{11}	103.46	104.16	C_5—C_6—C_7—O_{18}	115.18	124.30
N_8—C_{17}	1.4455	1.455	C_6—C_7—O_{18}	109.31	109.46	C_5—C_6—C_7—C_{11}	−5.85	1.30
C_{17}—H_{27}	1.0869	0.980	C_{11}—C_7—O_{18}	113.35	114.61	C_5—C_6—C_7—N_8	−116.64	−109.23
C_{17}—H_{28}	1.0935	0.980	N_8—C_7—O_{18}	113.05	112.49	C_6—C_5—C_{12}—C_{11}	10.62	4.12
C_{17}—H_{29}	1.0888	0.980	C_6—C_7—N_8	114.70	113.35	C_6—C_5—C_{12}—O_{13}	−166.57	−176.00
N_8—C_9	1.3770	1.356	C_{11}—C_7—N_8	102.48	102.42	C_6—C_7—O_{18}—H_{30}	−139.68	−168.79
C_{11}—N_{10}	1.4349	1.442	C_7—N_8—C_9	112.57	112.52	C_6—C_7—N_8—C_9	100.23	107.52
N_{10}—C_9	1.3892	1.366	C_7—N_8—C_{17}	124.57	124.27	C_6—C_7—N_8—C_{17}	−71.82	−65.78
C_9═O_{16}	1.2133	1.233	C_9—N_8—C_{17}	122.35	122.86	C_6—C_7—C_{11}—N_{10}	−105.12	−114.76
N_{10}—C_{15}	1.4496	1.454	N_8—C_9—N_{10}	107.50	109.21	C_6—C_7—C_{11}—O_{14}	132.89	126.01
C_{15}—H_{24}	1.0897	0.980	N_8—C_9—O_{16}	126.55	126.78	C_6—C_7—C_{11}—C_{12}	11.68	1.18
C_{15}—H_{25}	1.0919	0.980	N_{10}—C_9—O_{16}	125.94	124.00	C_7—N_8—C_{17}—H_{27}	−165.51	−150.75
C_{15}—H_{26}	1.0864	0.980	C_9—N_{10}—C_{11}	112.26	112.88	C_7—N_8—C_{17}—H_{28}	75.33	89.24
C_7—N_8	1.4466	1.460	C_9—N_{10}—C_{15}	121.97	123.48	C_7—N_8—C_{17}—H_{29}	−46.38	−30.70
			C_{11}—N_{10}—C_{15}	123.22	123.56	O_{13}—C_{12}—C_{11}—O_{14}	42.27	51.43
			C_{12}—C_{11}—C_7	105.27	105.17	O_{13}—C_{12}—C_{11}—C_7	163.64	−176.98
			C_{12}—C_{11}—N_{10}	111.42	110.71	C_{13}—C_{12}—C_{11}—N_{10}	−85.52	−72.65
			C_{12}—C_{11}—O_{14}	111.50	113.22	C_{12}—C_{11}—O_{14}—H_{23}	−20.82	13.65
			C_7—C_{11}—N_{10}	102.88	102.81	C_{12}—C_{11}—N_{10}—C_{15}	71.49	69.08
			C_7—C_{11}—O_{14}	111.75	114.36	C_{12}—C_{11}—N_{10}—C_9	−126.27	−114.04
			N_{10}—C_{11}—O_{14}	113.38	110.01	C_{12}—C_{11}—C_7—O_{18}	−106.59	−118.39
			C_{11}—C_{12}—O_{13}	123.22	124.13	C_7—C_{11}—O_{14}—H_{23}	−138.35	−106.81
			C_5—C_{12}—O_{13}	129.35	127.92	N_{10}—C_{11}—O_{14}—H_{23}	105.91	138.11
			C_5—C_{12}—C_{11}	107.36	107.95	N_8—C_7—O_{18}—H_{30}	−98.84	64.25
			C_{11}—O_{14}—H_{23}	107.83	112.37	C_{11}—C_7—O_{18}—H_{30}	−24.85	−52.22
			N_{10}—C_{15}—H_{24}	110.63	109.45	C_{11}—C_7—N_8—C_{17}	176.80	−177.38
			N_{10}—C_{15}—H_{25}	111.43	109.49	C_{11}—C_7—N_8—C_9	−11.13	−4.07
			N_{10}—C_{15}—H_{26}	107.32	109.49	C_{11}—N_{10}—C_{15}—H_{24}	−62.02	−58.69
			H_{24}—C_{15}—H_{25}	108.94	109.47	C_{11}—N_{10}—C_{15}—H_{25}	59.34	61.31
			H_{24}—C_{15}—H_{26}	109.45	109.49	C_{11}—N_{10}—C_{15}—H_{26}	178.61	−178.72
			H_{25}—C_{15}—H_{26}	109.00	109.43	C_{11}—N_{10}—C_9—O_{16}	−173.10	178.64
			N_8—C_{17}—H_{27}	107.79	109.53	C_{11}—N_{10}—C_9—N_8	7.61	−0.31
			N_8—C_{17}—H_{28}	112.32	109.43	N_{10}—C_9—N_8—C_7	3.07	−2.97
			N_8—C_{17}—H_{29}	109.65	109.45	N_{10}—C_9—N_8—C_{17}	175.33	−176.39
			H_{27}—C_{17}—H_{29}	109.49	109.53	C_9—N_8—C_7—C_{11}	−11.13	−4.07
			H_{27}—C_{17}—H_{28}	108.23	109.50	C_9—N_8—C_{17}—H_{27}	23.17	36.62
			H_{28}—C_{17}—H_{29}	109.28	109.46	C_9—N_8—C_{17}—H_{28}	−95.97	−83.39
			C_7—O_{18}—H_{30}	107.17	108.40	C_9—N_8—C_{17}—H_{29}	142.30	156.67

the usual value of 1.43 Å. The double bond character of C_9═O_{16} and C_{12}═O_{13} can be confirmed from the bond length of 1.21 Å due to the increase in electron density between the molecules. From the table, it is clear that the experimental results match well with the computed values.

4.4. Optical absorption studies

When energy corresponding to the ultraviolet–visible region is given to the molecule, the excitation of valence electrons from an occupied molecular orbital (bonding orbital or non-bonding p) causes transition to higher energy orbital (anti-bonding orbital) [26]. The high extinction coefficient for a molecule in the UV region represents wavelength of maximum absorption in the spectrum. According to the nature of the molecule and energy available, σ–σ^*, n–σ^*, π–π^* and n–π^* transitions are possible. For the present case, the experimental (in water) and simulated (in gas phase and water) UV–Vis spectra of the title compound are presented in Fig. 4. The solvent effect was calculated using the PCM–TD-DFT method for the HP and HLYP/cc-pVTZ basis set. Position and absorbance of the experimental peaks together with the calculated excitation energies, oscillator strength (f), wavelength (λ), and spectral assignments have been tabulated (Table S1; in Supplementary Material). From the table, the first dipole allowed transition is calculated at 294.99 nm (64A → 66A) in the water phase with oscillator strength of 0.006 and 301.97 nm (60A → 66A) in gas phase with oscillator strength of 0.0049. The transition with maximum oscillator strength [27] of 0.2410 occurs at

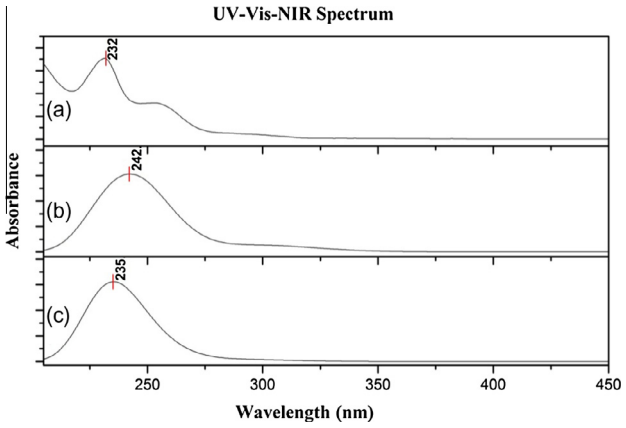

Fig. 4. (a) Experimental UV–Vis spectrum of NDUN, (b) simulated UV–Vis spectrum of NDUN in gas phase and (c) simulated UV–Vis spectrum of NDUN in water.

233.58 nm in water phase and in gas phase it occurs at 232.67 nm. The experimental absorption spectrum shows a strong transition at 232 nm, which matches well with the calculated value. From the spectrum, it is also evident that NDUN crystal has UV cut-off wavelength near 310 nm. This is due to the presence of hydroxyl and amino group in the title compound. This reduction in absorption has a significant contribution toward the resistance to laser induced damage. Thus the optical transmittance study shows that NDUN is a good candidate for NLO application.

The interaction of the molecule with other molecules can be determined from the Highest Occupied Molecular Orbitals (HOMO) and the Lowest Unoccupied Molecular Orbitals (LUMO) [28]. The difference in the energies of these levels gives the energy gap from which the chemical reactivity and the kinetics of the molecule can be studied. (HOMO and LUMO plots of NDUN and the energies of these orbitals in the gas and water phases are shown in Fig. S3 in Supplementary Material.)

In gas phase:	HOMO Energy	= −0.30397 a.u.
	LUMO Energy	= −0.04330 a.u.
	HOMO—LUMO Energy gap, ΔE	= −0.26067 a.u.
In water phase:	HOMO Energy	= −0.30531 a.u.
	LUMO Energy	= −0.04093 a.u.
	HOMO—LUMO Energy gap, ΔE	= −0.26438 a.u.

The small value of HOMO–LUMO energy gap indicates intramolecular charge transfer from the electron-donating group to the electron accepting group [29] and it aids nonlinear optical processes.

4.5. Natural bond orbital analysis

The interpretation of wavefunctions of atoms can be done chemically using natural bond orbital analysis (NBO). The presence of hydrogen bonding and the other intra or intermolecular charge transfer taking place in the molecule can be analyzed. Existence of intermolecular hydrogen bond O—H···O can be confirmed from the interaction between LP_2O_{14} and antibonding orbital $\sigma^*(O_{18}—H_{30})$ with a stabilization energy of 1.27 kcal/mol. Intramolecular charge transfer (ICT) which stabilizes the system are formed by the overlap of $\pi \rightarrow \pi^*$ bond orbitals in the intramolecular interactions. The energy density of the six conjugated π bonds of the phenyl rings shows strong delocalization giving a stabilization energy of ~20 kcal/mol. The orbital interaction energies of $LP_1(N_8) \rightarrow \sigma^*(C_9—O_{16})$ and $LP_1(N_{10}) \rightarrow \sigma^*(C_9—O_{16})$ are 37.62 kcal/mol and 33.02 kcal/mol respectively. These high interaction energies due to ICT interactions stabilize the molecule. Table 4 presents the tabulated results.

4.6. Thermal studies

Thermo-gravimetric analysis (TGA) is a technique in which the mass of a substance is monitored as a function of temperature as the sample is subjected to a controlled temperature program. It is used to find the thermal stability of the material. For a thermally stable material, there will be no observed mass change and will not show any slope in the TGA curve [30]. TGA also gives the upper temperature beyond which the material will begin to degrade, as a descending TGA curve where weight loss is occurred. In the TG/DTA curves given in Fig. 5, for NDUN, the extrapolated onset temperature that denotes the temperature at which the weight loss begins is 268.08 °C. The inflection point which is the first derivative of the weight loss curve is 271.64 °C. It indicates the point of greatest rate of change on the weight loss curve. The TG curve shows a weight decrease of 88.77% from a temperature of 268.08–296.08 °C. The DTA curve shows an endothermic peak at 279 °C which is attributable to the desorption of adsorbed water.

4.7. Z-scan studies

The tetragonal urea crystal [3], being a non-centrosymmetric organic material, is known to be used as a standard for measuring second harmonic generation by Kurtz–Perry technique. The ninhydrin molecule also shows second order nonlinearity [31] along with third order nonlinear optical (NLO) behaviour. The third order NLO property of ninhydrin is due to effective 2PA mechanism and the respective coefficient obtained from the best numerical fit to the data is 5.0×10^{-11} m/W [32]. From XRD data, NDUN is found to be a centrosymmetric material and shows only third order NLO property.

The experimental z-scan data obtained (shown as open circles) are numerically fitted to the nonlinear transmission equation for a two-photon absorption process, given by,

$$T = \left((1-R^2)\frac{\exp(-\alpha_0 L)}{\sqrt{\pi q_0}}\right)\int_{-\infty}^{+\infty} In[1+q_0\exp(-t^2)]dt \qquad (6)$$

where T is the normalized transmission of the sample. L is the length, R is the surface reflectivity, and α_0 is the linear absorption coefficient of the sample. $q_0 = \beta(1-R)I_0L_{eff}$ where I_0 is the on-axis peak laser intensity, and β is the two-photon absorption coefficient. $L_{eff} = [1-\exp(-\alpha_0 L)]/\alpha_0$ is the effective length of the sample.

The open aperture Z-scan curve [33] of NDUN is given in Fig. 6a, and the nonlinear transmission curve calculated from the Z-scan data is given in Fig. 6b, respectively. A decrease in sample transmittance is observed when the input light fluence is increased.

The observed nonlinearity which numerically fits to two-photon absorption in fact originates mostly from two-step excitation (excited state absorption). Therefore the nonlinearity can be considered as an "effective" two-photon absorption process. Such absorptive nonlinearities involving real excited states have been reported earlier in C_{60} (fullerenes), metal nanoclusters, semiconductors, porphyrins, etc. [34–40]. The effective 2PA coefficient calculated for NDUN from the best numerical fit to the data is 4.25×10^{-11} m/W. In comparison, values of 9×10^{-11} m/W and 23×10^{-11} m/W were obtained in polyaniline and polyaniline–porphyrin nanocomposites, [41] and 30×10^{-11} m/W in a copolymer containing oxadiazole and substituted thiophene [42], under similar excitation conditions. The sample shows linear transmittance of about 70%.

Table 4
NBO analysis based on second-order perturbation theory.

Donor (i)	Natural orbital occupancy (ED_i)	Acceptor (j)	Natural orbital occupancy (ED_j)	Energy density[a] $E(2)$ (kcal/mol)	[b]$E(j) - E(i)$ (a.u.)	[c]$F(ij)$ (a.u.)
$\pi(C_1—C_2)$	1.64460	$\pi^*(C_3—C_4)$	0.27418	17.59	0.28	0.064
$\pi(C_1—C_2)$	1.64460	$\pi^*(C_5—C_6)$	0.38308	23.72	0.29	0.074
$\pi(C_3—C_4)$	1.66083	$\pi^*(C_1—C_2)$	0.29583	21.08	0.28	0.070
$\pi(C_3—C_4)$	1.66083	$\pi^*(C_5—C_6)$	0.38308	19.04	0.29	0.067
$\pi(C_5—C_6)$	1.61476	$\pi^*(C_1—C_2)$	0.29583	17.03	0.28	0.063
$\pi(C_5—C_6)$	1.61476	$\pi^*(C_3—C_4)$	0.27418	19.47	0.28	0.068
$\pi(C_5—C_6)$	1.61476	$\pi^*(C_{12}—O_{13})$	0.16251	25.32	0.27	0.078
$LP_1(N_8)$	1.70975	$\sigma^*(C_9—O_{16})$	0.35678	37.62	0.38	0.107
$LP_1(N_{10})$	1.72640	$\sigma^*(C_9—O_{16})$	0.35678	33.02	0.39	0.102
$LP_1(N_{10})$	1.72640	$\sigma^*(C_{11}—O_{14})$	0.05921	13.35	0.53	0.080
$LP_2(O_{13})$	1.86956	$\sigma^*(C_5—C_{12})$	0.07266	21.06	0.72	0.111
$LP_2(O_{13})$	1.86956	$\sigma^*(C_{11}—C_{12})$	0.10397	23.54	0.62	0.109
$LP_2(O_{14})$	1.93019	$\sigma^*(N_{10}—C_{11})$	0.06159	11.92	0.68	0.080
$LP_2(O_{16})$	1.83574	$\sigma^*(N_8—C_9)$	0.09015	25.88	0.68	0.121
$LP_2(O_{16})$	1.83574	$\sigma^*(C_9—N_{10})$	0.09588	26.65	0.66	0.121
$LP_2(O_{18})$	1.93017	$\sigma^*(C_7—N_8)$	0.07191	12.91	0.65	0.082
$LP_1(O_{14})$	1.97208	$\sigma^*(O_{18}—H_{30})$	0.01670	0.75	1.05	0.025
$LP_2(O_{14})$	1.93019	$\sigma^*(O_{18}—H_{30})$	0.01670	1.27	0.76	0.028

[a] $E(2)$ – Energy of hyperconjugative interactions.
[b] $E(j) - E(i)$ – Energy difference between donor (i) and acceptor (j) NBOs.
[c] $F(ij)$ – Fock matrix element.

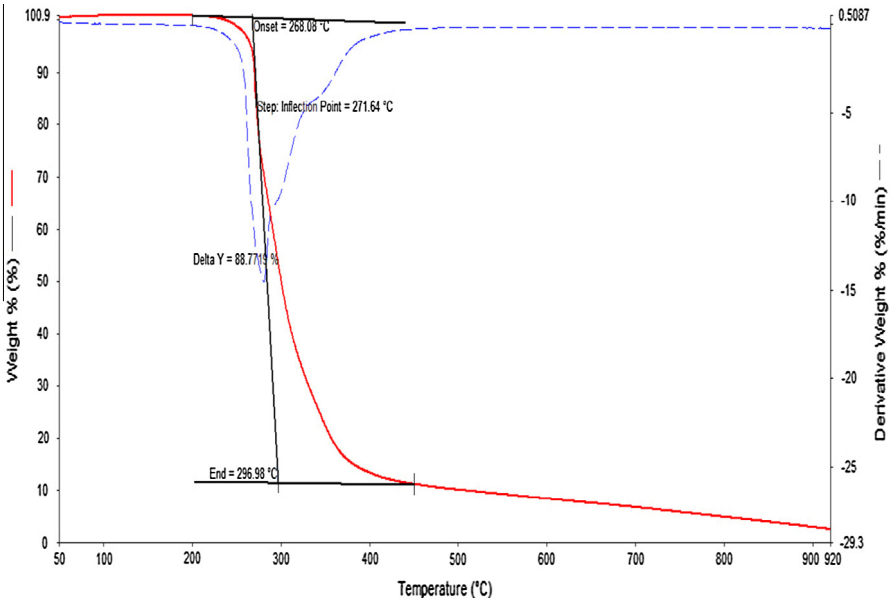

Fig. 5. TG/DTA curves.

4.7.1. Hyperpolarizability calculations

The experimental data of first hyperpolarizability obtained from the EFISH (electric-field-induced second harmonic generation) measurement in water solution for urea is $(0.45 \pm 0.12) \times 10^{-30}$ e.s.u. [43], which ranges from 0.33×10^{-30} to 0.57×10^{-30} e.s.u. (38–66 a.u.). The values taken from the Gaussian'09 output for calculation of first hyperpolarizability of NDUN molecule are given in Table S2 (in Supplementary Material). The static first hyperpolarizability value of NDUN molecule is calculated to be 4.55×10^{-30} e.s.u., which is 6.68 times larger than that of urea. Since the molecule is centrosymmetric, experimentally no second order NLO properties are shown by the molecule. The second hyperpolarizability value, which is a measure of third order NLO properties, obtained for NDUN is 21.857×10^{-36} e.s.u. The linear polarizability value for the molecule is found to be 24.244×10^{-24} e.s.u.

4.8. Vibrational spectral analysis

In the vibrational analysis of NDUN, the potential energy distributions (PEDs) reveal that many of the internal modes contribute to a particular vibrational mode and involve the simultaneous motion of a large number of atoms. The non-redundant sets of internal coordinates for NDUN have been defined in Table S3 (in Supplementary Material). Selective scaling was done using a set of 11 transferable scale factors giving an RMS wavenumber 9.46 cm^{-1}. The observed and calculated wavenumbers together with the Infrared and Raman intensities and normal modes description (characterized by PED) of NDUN are reported in Table 5. A comparison of the observed and simulated IR and FT-Raman spectra of the title compound are presented in Figs. 7a and 7b, which helps to understand the observed spectral features.

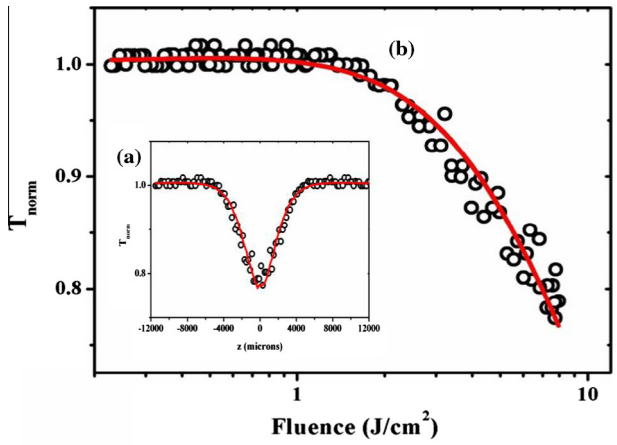

Fig. 6. (a) Open aperture Z-scan curve measured for the sample. Circles are data points while the solid curve is a numerical fit to Eq. (6). (b) Variation of normalized transmittance with input laser fluence, calculated from the Z scan data using Eq. (1). Circles are data points while solid curve is a numerical fit using Eqs. (1) and (6).

The calculated spectra were found to be close to the experimental values with reasonable accuracy. H-atoms involved in intermolecular H-bonds give rise to deviations of the simulated spectra from the experimental spectra, which is attributed to the fact that the theoretical spectrum was obtained in gas phase without considering the intermolecular H-bonding effects.

4.8.1. OH vibrations

OH vibrations are generally observed in the region 3200–3600 cm^{-1} [44]. The value of OH stretching frequency can be used as a test for and measure of the strength of hydrogen bonds. There is a medium strong IR peak at 3304 cm^{-1} with potential energy distribution (PED) of 100% for OH (O_{14}—H_{23}) stretching. The higher intensity than a free OH vibration indicates the presence of an intramolecular hydrogen bonding. In the theoretical IR spectra we can observe a peak at 3280 cm^{-1} formed due to the other OH group present in NDUN. A very weak peak at 408 cm^{-1} (PED 50%), in the Raman spectrum, is due to the torsional oscillation of the two OH groups, which usually appears in the region 350–450 cm^{-1}.

4.8.2. Methyl group vibrations

The molecule consists of two methyl groups each having three CH bonds that participate in the stretching vibrations. In the symmetric in-phase stretching vibration, the whole CH_3 group is stretching in phase. The two out-of-phase stretching vibrations can be simply characterized as half-methyl stretch. There are three HCH angles and three HCH bending vibrations in the methyl group. The bending vibrations are described as a symmetric, in-phase CH_3 deformation and two degenerate or nearly degenerate out-of-phase half-methyl deformations. CH_3 in-plane stretching vibration with a PED of 92% is observed as a weak peak at 3042 cm^{-1} in the IR spectrum. A very weak peak at 2949 cm^{-1} in the IR spectrum is contributed by CH_3 out of plane stretching with a PED of 65% and

Table 5
Calculated wavenumbers, experimental peak positions in IR and Raman spectra and the assignments for NDUN molecule for basis set B3LYP/cc-pVTZ are tabulated.

Calculated wavenumbers	Experimental wavenumbers		IR intensity (in 100)	Raman intensity (in 100)	PED (%)
Scaled (cm^{-1})	ν_{IR} (cm^{-1})	ν_{Raman} (cm^{-1})			
3303	3304 ms		10.9	14.0	OH (100)
3280			15.7	18.4	OH (100)
3093	3107 w		2.27	74.3	CH (99)
3088	3090 w	3087 vw	2.63	63.4	CH (99)
3076	3069 w		1.34	42.4	CH (99)
3062	3057 w	3059 w	0.51	23.4	CH (99)
3023	3042 w		0.47	22.7	CH_3IPS (92)
2954	2949 vw		4.24	33.1	CH_3OPS (65), CH_3SS (34)
1729	1729 ms	1723 vs	100	5.53	CODOU (70), CN (21)
1678	1678 vs		50.5	100	CODOU (74), bRING2 (10), CC (10)
	1682 vs				
1605	1604 w	1605 s	11.6	56.5	CC (63), bCH (17), bRING1 (15)
1588		1590 s	1.73	43.3	CC (55), bRING1 (13), bCH (13), bCCC (12)
1488	1488 ms		32.5	5.84	CN (25), CH_3OPB (15), bCH (14)
1455	1461 s		7.86	22.2	CH_3IPB (50), CH_3OPR (20), CH_3OPB (16)
	1464 s				
1414	1418 s		7.69	4.04	CH_3SB (78)
1399	1399 ms		10.9	8.39	CH_3SB (67)
1355			4.44	7.84	CC (47)
1302	1295 w		5.49	14.0	bCH (46), CC (23), gCO (10)
1274	1264 s		7.11	23.5	CC (24), CH_3OPR (22), CH_3IPB (12)
	1272 s				
1247	1241 vw	1240 w	3.39	21.1	CH_3OPR (20), CC (15), CH_3IPB (14), bOCC (13)
1212	1212 ms		7.54	21.3	CH_3OPR (19), CC (16), bCO (11)
1171	1183 s	1183 w	1.98	16.5	bCH (47), CC (21)
1167	1170 ms		1.93	13.1	CC (26), bCH (19), gCO (14), bCO (10)
	1154 w				
1078	1078 s		4.94	16.8	CH_3IPR (17), bCOH (15), bRING1 (11), COSIN (11)
1042	1035 ms		9.11	12.5	CH_3IPR (23), bRING1 (22), CC (15)
1020		1022 w	6.78	77.7	CC (53), bCH (12), bCOH (10)
981	982 w	982 vw	5.33	2.90	gCH (87)
930	942 w		8.45	17.2	bRING1 (21), bCO (14), COSIN (12)
859	860 w		5.59	10.5	CC (23), bCO (21), bCOH (20)
766	747 s		8.67	1.72	gCH (29), gCO (23), bOCC (17), bCO (11)
	768 s				
666	667 s	670 s	2.32	11.6	bRING1 (29), tRING1 (20)
578	577 w		0.98	16.4	gCO (26), tRING1 (20)
556	544 w	551 vw	2.15	18.3	NC (44), bRING3 (20)
532		536 s	1.38	59.4	bRING1(30), bRING2(19), CC (16)
415		408 vw	9.02	17.2	tOH (50), tRING1 (11)

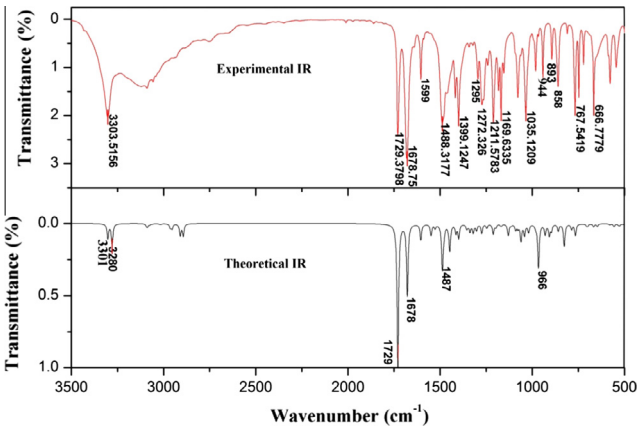

Fig. 7a. Experimental and theoretical FT-IR Spectra combined.

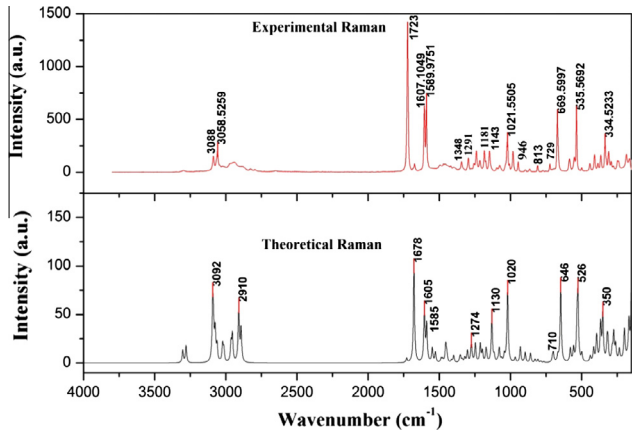

Fig. 7b. Experimental and theoretical FT-Raman spectra combined.

CH_3 symmetric stretch with PED% of 34. Two strong peaks at 1461 cm^{-1} and 1464 cm^{-1} in the IR spectrum can be attributed to the combined CH_3 vibrations of in-plane bending (PED 50%), out-of-plane rocking (PED 20%) and out-of-plane bending (PED 16%). CH_3 symmetric bending peaks can be observed at 1418 cm^{-1} as a strong peak (PED 78%) and at 1399 cm^{-1} as a medium strong peak (PED 67%) in the IR spectrum. CH_3 in-plane bending vibrations can be observed as peaks at 1272 and 1241 cm^{-1} in the IR spectrum. A medium strong band at 1488 cm^{-1} in the IR spectrum can be assigned to CH_3 out-of-plane bending vibrations. The CH_3 out-of-plane rocking vibrations form peaks at 1264 cm^{-1}, 1241 cm^{-1} and 1212 cm^{-1} in the IR spectrum. In-plane rocking vibrations of CH_3 molecule are observed at 1078 cm^{-1} and 1035 cm^{-1} in IR spectrum.

4.8.3. C═O vibrations

The carbonyl stretching vibrations generally occur in the region 1650–1750 cm^{-1}. The medium strong band at 1729 cm^{-1} and strong peak at 1678 cm^{-1} in the FT-IR spectrum matches exactly with the theoretical values for C═O stretching vibrations with PED of 70 and 74% respectively. There is a corresponding strong peak at 1723 cm^{-1} in the FT-Raman spectrum.

4.8.4. Ring vibrations

The three rings in NDUN are benzene (ring 1), cyclopentane (ring 2) and imidazole (ring 3).

For the hetero aromatic structure the CH stretching vibrations can be found in the region 3100–3000 cm^{-1}. The weak peaks at 3107, 3090, 3069 and 3057 cm^{-1} in the IR and at 3087 and 3059 cm^{-1} in the Raman spectra are attributed to CH stretching vibrations of ring 1 with a PED of 99%. Since the bands in this region are not affected by the nature of substitutes, the peaks match with that of ninhydrin molecule. According to Wilson's numbering convention there are four CH stretching vibration modes which include modes 2, 7, 13 and 20 [45]. The active modes in o-disubstituted benzene ring are 2, 7b, 20a and 20b. The weak peak at 3107 cm^{-1} in the IR spectrum with 3093 cm^{-1} as the theoretical value is assigned to mode 2 according to the vibrations of CH bonds in NDUN. The peaks at 3090 cm^{-1} in the IR and 3087 cm^{-1} in the Raman spectra can be assigned to mode 20a which usually has the range 3050–3090 cm^{-1}. A peak is seen at 3069 cm^{-1} in the IR which is assigned as mode 20b, normally occurring between 3020 and 3120 cm^{-1}. Peaks at 3057 cm^{-1} in IR and 3059 cm^{-1} in Raman spectra are assigned to mode 7b whose usual range is 3030–3050 cm^{-1}. Due to charge transfer mechanism between carbon and hydrogen atoms, these peaks are observed to be weak. The atomic movements included in the different CH stretching modes are shown in Table S4 (in Supplementary Material).

The peaks of C—H in-plane bending vibrations for aromatic compounds occur in the regions 1000–1300 cm^{-1}. The weak band at 1295 cm^{-1} due to C—H in-plane bending can be assigned to mode 3 with frequency range 1272–1292 cm^{-1}. CH in-plane bending vibrational peak detected at 1183 cm^{-1} simultaneously in IR and Raman spectra shows the internal charge transfer. This peak is of the type of mode 9a. A medium strong band at 1035 cm^{-1} in the IR spectrum is partially contributed by the CH in-plane bending vibration (PED 22%).

Carbon–Carbon stretching vibrations occur in the region 1000–1600 cm^{-1}. Strong bands at 1605 and 1590 cm^{-1} in the Raman spectra are assigned to the CC stretching vibrations. A weak peak at 942 cm^{-1} shows the C—C—C bending vibration of ring 1 with a PED of 21%. A strong peak at 667 cm^{-1} in the IR and 670 cm^{-1} in the Raman spectra is formed due to the combined bending (PED 29%) and torsional (PED 20%) vibrations of the ring. A strong peak at 536 cm^{-1} in the Raman spectrum is also contributed by the bending vibrations of benzene ring (PED 30%). The C—C—C—H torsional oscillations of benzene ring are observed at 982 cm^{-1} in the IR and Raman spectra.

The combined bending vibrations of ring1 and ring 2 are observed at 536 cm^{-1} in the Raman spectrum. NC (N_8—C_{17} and N_{10}—C_{15}) vibrations of the third ring are observed at 544 and 551 cm^{-1} of IR and Raman spectra respectively. The torsional oscillations of the second and third rings are mostly observed below 200 cm^{-1}.

5. Conclusion

A detailed study of a newly synthesized organic material, N, N′dimethylurea ninhydrin (NDUN), has been carried out. Employing slow evaporation method, the crystals were grown from the solution. The crystal structure of NDUN was determined by single crystal X-ray diffraction analysis which reveals that the crystal belongs to triclinic system. The compound has hydrogen atoms in the two methyl groups, two hydroxyl groups, and also attached to the carbon atoms; all the protons have shown their presence in the ^1H NMR spectrum. A peak at 232 nm has been observed in the theoretical and experimental UV–Vis spectra. A small value of HOMO–LUMO energy gap gives evidence for intramolecular charge transfer. Optical nonlinearity was studied by employing the open-aperture Z-scan technique. The nonlinear absorption coefficient of the NDUN molecule has been numerically calculated. Theoretical simulation of first and second

hyperpolarizability values were carried out. The detailed interpretation of the vibrational spectra has been done with the aid of normal coordinate analysis. FTIR and FT-Raman spectra of NDUN have been recorded and analyzed.

Acknowledgements

J.S.J.(Jerin Susan John) thanks the University Grants Commission – India (UGC) for funding the minor research project (Letter No. MRP(S)-1388/11-12/KLKE002/UGC-SWRO). P.S. (Pranitha Sankar) is grateful to the Australia-India Strategic Research Fund (AISRF) for a junior research fellowship.

Appendix A. Supplementary material

Supplementary data associated with this article can be found, in the online version, at http://dx.doi.org/10.1016/j.optmat.2015.08.002.

References

[1] G.S. He, B.A. Reinhardt, J.C. Bhatt, A.G. Dillard, G.C. Xu, P.N. Prasad, Opt. Lett. 20 (1995) 435–437.
[2] R.T. Edward Tiekink, Jagadese Vittal, Michael Zaworotko, Organic Crystal Engineering: Frontiers in Crystal Engineering, John Wiley & Sons Ltd., United Kingdom, 2010.
[3] F. David Eaton, Science 253 (1991) 281–285.
[4] M. Arivazhagan, D. Anitha Rexalin, Spectrochim. Acta Part A Mol. Biomol. Spectrosc. 109 (2013) 331–343.
[5] Hans Berger, Hans-Arthur Bradaczek, Hans Bradaczek, J. Mater. Sci.: Mater. Electron. 19 (2008) 351–355.
[6] M. Sheik-Bahae, A.A. Said, T.M. Wei, D.J. Hagan, E.W. Van-Stryland, IEEE J. Quant. Electron. 26 (1990) 760.
[7] S. Sreeja, S. Sreedhanya, N. Smijesh, Reji Philip, C.I. Muneera, J. Mater. Chem. C 1 (2013) 3851.
[8] M.J. Frisch, G.W. Trucks, H.B. Schlegel, G.E. Scuseria, M.A. Robb, J.R. Cheeseman, J.A. Montgomery Jr., T. Vreven, K.N. Kudin, J.C. Burant, J.M. Millam, Iyengar, J. Tomasi, V. Barone, B. Mennucci, M. Cossi, G. Scalmani, N. Rega, G.A. Petersson, H. Nakatsuji, M. Hada, M. Ehara, K. Toyota, R. Fukuda, J. Hasegawa, M. Ishida, T. Nakajima, Y. Honda, O. Kitao, H. Nakai, M. Klene, X. Li, J.E. Knox, H.P. Hratchian, J.B. Cross, V. Bakken, C. Adamo, J. Jaramillo, R. Gomperts, R.E. Stratmann, O. Yazyev, A.J. Austin, R. Cammi, C. Pomelli, J.W. Ochterski, P.Y. Ayala, K. Morokuma, G.A. Voth, P. Salvador, J.J. Dannenberg, V.G. Zakrzewski, S. Dapprich, A.D. Daniels, M.C. Strain, O. Farkas, D.K. Malick, A.D. Rabuck, K. Raghavachari, J.B. Foresman, J.V. Ortiz, Q. Cui, A.G. Baboul, S. Clifford, J. Cioslowski, B.B. Stefanov, G. Liu, A. Liashenko, P. Piskorz, I. Komaromi, R.L. Martin, D.J. Fox, T. Keith, M.A. Al-Laham, C.Y. Peng, A. Nanayakkara, M. Challacombe, P.M.W. Gill, B. Johnson, W. Chen, M.W. Wong, C. Gonzalez, J.A. Pople, Gaussian 09, Revision B. 01, Gaussian Inc, Wallingford CT, 2010.
[9] A.D. Becke, Phys. Rev. A 38 (1988) 3098–3100.
[10] C. Lee, W. Yang, R.G. Parr, Phys. Rev. B 37 (1988) 785–789.
[11] E.D. Glendening, J.K. Badenhoop, A.E. Reed, J.E. Carpenter, J.A. Bohmann, C.M. Morales, F. Weinhold, NBO 5.0, Theoretical Chemistry Institute, University of Wisconsin, Madison, 2001.
[12] F. Weinhold, Nature 411 (2001) 539–541.
[13] F. Weinhold, C.R. Landis, Valency and Bonding: A Natural Bond Orbital Donor–Acceptor Perspective, Cambridge University Press, Cambridge, 2005.
[14] G. Rauhut, P. Pulay, J. Phys. Chem. 99 (1995) 3093.
[15] T. Sundius, J. Mol. Struct. 218 (1990) 321–326.
[16] T. Sundius, Vib. Spectrosc. 29 (2002) 89–95.
[17] G. Fogarasi, X. Zhou, P. Taylor, P. Pulay, J. Am. Chem. Soc. 114 (1992) 8191–8201.
[18] P. Pulay, G. Fogarasi, F. Pang, E. Boggs, J. Am. Chem. Soc. 101 (1979) 2550–2560.
[19] P. Pulay, G. Fogarasi, G. Pongor, J.E. Boggs, A. Vargha, J. Am. Chem. Soc. 105 (1983) 7037–7047.
[20] K.S. Thanthiriwatte, K.M. Nalin de Silva, J. Mol. Struct. (Theochem) 617 (2002) 169–175.
[21] Demetrios Xenides, George Maroulis, Chem. Phys. Lett. 319 (2000) 618–624.
[22] M. ElSayed Shalaby, M. Aisha Moustafa, S. Adel Girgis, M. Aida ElShaabiny, J. Crystallogr. 2014 (2014) 7.
[23] D.A. Skoog, F.J. Holler, S.R. Crouch, Principles of Instrumental Analysis, Thomson Brooks/Cole, USA, 2007.
[24] A.S. Helmy, Opt. Express 14 (2006) 1243–1252.
[25] H. Dudley Williams, Ian Fleming, Spectroscopic Methods in Organic Chemistry, fourth ed., Tata McGraw-Hill, London, 1989.
[26] P.S. Kalsi, Spectroscopy of Organic Compounds, sixth ed., New Age International (P) Ltd., New Delhi, 2004.
[27] W.E. Spicer, Phys. Rev. 112 (1958) 114.
[28] C. Meganathan, S. Sebastian, M. Kurt, Keun Woo Lee, N. Sundaraganesan, J. Raman Spectrosc. 41 (2010) 1369–1378.
[29] T. Vijayakumar, I. Hubert Joe, C.P. Reghunadhan Nair, V.S. Jayakumar, Chem. Phys. 343 (2008) 83–99.
[30] H.H. Horowitz, Gershon Metzger, Anal. Chem. 35 (1963) 1464–1468.
[31] T. Uma Devi, N. Lawrence, R. Ramesh Babu, K. Ramamurthi, G. Bhagavannarayana, Spectrochim. Acta Part A 71 (2009) 1667–1672.
[32] D. Sajan, T. Uma Devi, K. Safakath, Reji Philip, Ivan Nemec, M. Karabacak, Spectrochim. Acta Part A Mol. Biomol. Spectrosc. 109 (2013) 331–343.
[33] R.K. Choubey, R. Trivedi, M. Das, P.K. Sen, P. Sen, S. Kar, K.S. Bartwal, R.A. Ganeev, J. Cryst. Growth 311 (2009) 2597–2601.
[34] S. Couris, E. Koudoumas, A.A. Ruth, S.J. Leach, J. Phys. B: At. Mol. Opt. Phys. 28 (1995) 4537.
[35] R. Philip, G. Ravindra Kumar, N. Sandhyarani, T. Pradeep, Phys. Rev. B 62 (2000) 13160.
[36] L. Irimpan, V.P.N. Nampoori, P. Radhakrishnan, B. Krishnan, A.J. Deepthy, J. Appl. Phys. 103 (2008) 033105.
[37] I. Cohanoschi, M. Garci, C. Toro, F.K.D. Belfield, F.E. Hernandez, Chem. Phys. Lett. 430 (2006) 133.
[38] P. Wang, H. Ming, J. Xie, W. Zhang, X. Gao, Z. Xu, X. Wel, Opt. Commun. 192 (2001) 387.
[39] S. Medhekar, R. Kumar, S. Mukherjee, R.K. Choubey, AIP Conf. Proc. 1512 (2013) 470.
[40] R.K. Choubey, S. Medhekar, R. Kumar, S. Mukherjee, Sunil Kumar, J. Mater. Sci.: Mater. Electron. 25 (2014) 1410.
[41] R.K. Pandey, C.S. Suchand Sandeep, R. Philip, V.J. Lakshminarayanan, J. Phys. Chem. C 113 (2009) 8630.
[42] A.J. Kiran, D. Udayakumar, K. Chandrasekaran, A.V. Adhikari, H.D. Shashikala, R. Philip, Opt. Commun. 271 (2007) 236.
[43] Ledoux, J. Zyss, Chem. Phys. 73 (1983) 203–213.
[44] N.B. Colthup, L.H. Daly, S.E. Wiberley, Introduction to Infrared and Raman Spectroscopy, third ed., Academic Press, London, 1990.
[45] G. Varsanyi, Vibrational Spectra of Benzene Derivatives, first ed., Academic Press, New York and London, 1969.